arXiv:1210.4702v1 [astro-ph.SR] 17 Oct 2012

ACTA ASTRONOMICA
Vol. **62** (2012) pp. 247–268

Photometric Maps Based on the OGLE-III Shallow Survey in the Large Magellanic Cloud*

K. Ulaczyk[1], M.K. Szymański[1], A. Udalski[1],
M. Kubiak[1], G. Pietrzyński[1,2], I. Soszyński[1],
Ł. Wyrzykowski[1,3], R. Poleski[1],
W. Gieren[2], A.R. Walker[4] and A. Garcia-Varela[5]

[1] Warsaw University Observatory, Al. Ujazdowskie 4, 00-478 Warszawa, Poland
e-mail: (kulaczyk,msz,udalski,mk,pietrzyn,soszynsk,wyrzykow,rpoleski)@astrouw.edu.pl

[2] Universidad de Concepción, Departamento de Astronomia, Casilla 160-C, Concepción,
Chile
e-mail: wgieren@astro-udec.cl

[3] Institute of Astronomy, University of Cambridge, Madingley Road, Cambridge
CB3 0HA, UK

[4] Cerro Tololo Inter-American Observatory, Casilla 603, La Serena, Chile
e-mail: awalker@ctio.noao.edu

[5] Departamento de Fisica, Universidad de los Andes, Bogota, Colombia
e-mail: josegarc@uniandes.edu.co

Received October 1, 2012

ABSTRACT

We present photometric maps based on data from the shallow survey in the Large Magellanic Cloud performed as the supplementary project during the third phase of the Optical Gravitational Lensing Experiment. They cover about 40 square degrees in the LMC and contain mean calibrated *VI* photometry and astrometry of about 1.7 million stars. The magnitudes of the registered objects range from 9.1 to 18.5.

We discuss the quality of data and present color–magnitude diagrams of selected fields. The maps together with the main LMC photometric maps are available to the astronomical community from the OGLE Internet archive.

Key words: *Magellanic Clouds – Surveys – Catalogs – Techniques: photometric*

---

[*] Based on observations obtained with the 1.3 m Warsaw telescope at the Las Campanas Observatory of the Carnegie Institution for Science.

1. Introduction

The extensive OGLE-III Photometric Maps of the Large Magellanic Cloud have already been published in Udalski *et al.* (2008b). They contained stars as faint as 20.5 mag in *I*-band and showed high level of completeness. However, these maps suffered from obvious limitation – very bright objects became saturated during regular observations (performed with exposure times equal to 180 s and 240 s in *I*- and *V*-band, respectively). Typically, overexposure took place at $12.5 \div 13$ mag in the *I*-band, depending on stellar density. Obviously, numerous fainter stars registered on images in the vicinity of saturated objects could also be affected.

The main purpose of the shallow survey described in this paper was to complement the OGLE-III databases for the studied fields with objects for which photometry had not been previously obtained due to saturation in single or both bands. Here we describe reduction procedures applied to the collected short-exposure images, we present photometric maps for the Large Magellanic Cloud and we discuss quality of the data.

Table 1

Number of observations per field

Field	N_I	N_V	Field	N_I	N_V	Field	N_I	N_V	Field	N_I	N_V
LMC100	65	63	LMC131	22	22	LMC157	25	25	LMC190	20	20
LMC101	59	58	LMC132	21	21	LMC158	25	24	LMC191	51	51
LMC102	57	58	LMC133	86	83	LMC159	63	64	LMC192	51	50
LMC103	57	56	LMC134	81	80	LMC160	63	62	LMC193	50	50
LMC104	54	53	LMC135	80	78	LMC161	61	61	LMC194	20	20
LMC105	52	52	LMC136	78	78	LMC162	57	57	LMC195	20	20
LMC107	78	78	LMC137	21	21	LMC163	57	54	LMC196	21	21
LMC108	77	77	LMC138	26	26	LMC164	55	55	LMC197	21	21
LMC109	74	75	LMC139	26	26	LMC165	54	54	LMC198	21	21
LMC110	75	75	LMC140	26	25	LMC167	60	59	LMC199	21	21
LMC111	73	72	LMC141	25	25	LMC168	57	57	LMC200	21	20
LMC112	69	70	LMC142	25	25	LMC169	57	56	LMC201	19	19
LMC113	70	69	LMC143	25	25	LMC170	55	55	LMC202	19	19
LMC114	68	67	LMC144	25	25	LMC171	55	55	LMC203	19	19
LMC117	72	73	LMC145	26	26	LMC172	53	52	LMC204	17	17
LMC118	73	73	LMC146	26	26	LMC174	59	60	LMC205	17	17
LMC119	72	72	LMC147	26	26	LMC175	59	57	LMC206	17	17
LMC120	72	72	LMC148	25	25	LMC176	59	59	LMC207	15	15
LMC121	71	69	LMC149	25	24	LMC177	55	55	LMC208	15	15
LMC124	82	81	LMC150	25	25	LMC178	58	57	LMC209	14	14
LMC125	81	80	LMC151	25	25	LMC179	58	56	LMC210	14	14
LMC126	80	78	LMC152	30	30	LMC183	63	62	LMC211	14	14
LMC127	78	77	LMC153	28	28	LMC184	58	57	LMC212	13	13
LMC128	75	75	LMC154	26	25	LMC185	58	58	LMC213	13	13
LMC129	72	72	LMC155	26	26	LMC186	56	56	LMC214	13	13
LMC130	69	69	LMC156	26	26	LMC189	20	20	LMC215	13	12

2. Observations

Observational data were collected using 1.3-m Warsaw Telescope located at Las Campanas Observatory, operated by the Carnegie Institution for Science. During the third phase of the OGLE project the telescope was equipped with the eight chip mosaic camera covering approximately $35' \times 35'$ field of view with the scale of 0.26 arcsec/pixel. The *I* and *V* filters used in the survey closely resembled standard filters, although *I*-band filter had higher transmission for longer wavelengths. Detailed description of the whole instrumentation can be found in Udalski (2003). We also used data from OGLE-IV survey to correct the photometry of red objects.

Images were registered during nights of seeing worse then about $2''$. It allowed to blur profiles of the brightest stars preventing from the saturation. Moreover we were able to perform observations during nights of poor weather which normally would be lost for the main OGLE survey.

Typical exposure time was equal to 15 s for both filters. A process of camera shutter opening took about 0.3 s so the possible shutter error was negligible. For a period of 4.5 years total amount of 74 192 subfield images were registered through both filters. Table 1 and diagram in Fig. 1 present number of observations available for each field. The standard OGLE-III field designations were used as described in Udalski *et al.* (2008b).

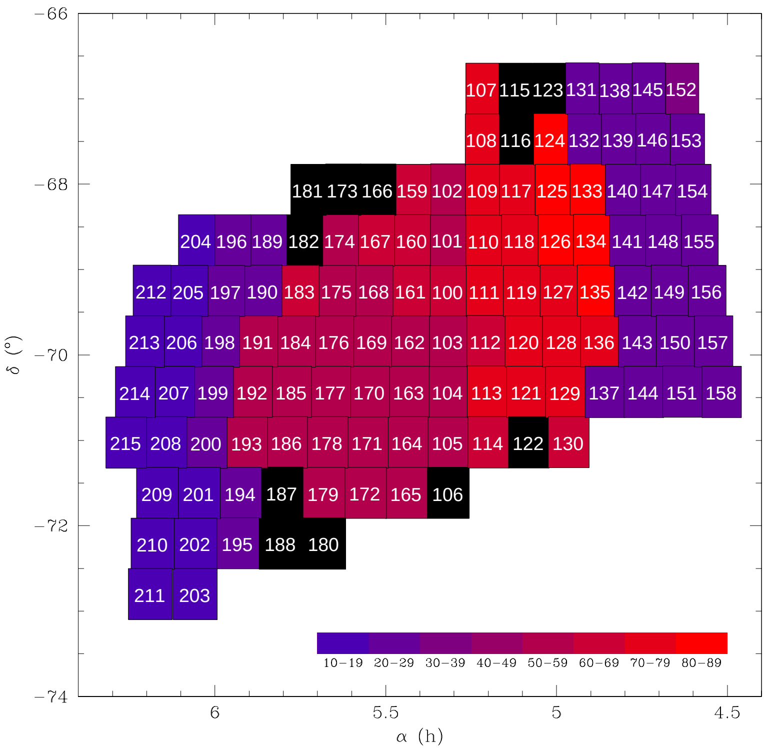

Fig. 1. Number of observations per field. The black color means "no observations".

3. Data Reductions

Preliminary reductions of all images – debiasing and flatfielding – were performed immediately after collecting at the telescope using the standard OGLE pipelines (Udalski 2003).

In order to minimize PSF variability each subfield image (corresponding to one camera chip) was divided into two parts with overlapping region of 40 pixels.

Then profile photometry with DAOPHOT/ALLSTAR package (Stetson 1987) was performed for all obtained 2048×2068 images. PSF profiles were derived from at least 15 isolated stars selected from initial list of 30 objects filtered by rejecting 3σ deviations from the model. For all images database was constructed consisting of photometric measurements in the *I*- and *V*-band as well as a position data.

The linear shifts in (X,Y) coordinates between subsequent images of the same photometric subfield were derived and for all detected objects light curves were prepared. The small inaccuracies of the telescope pointing allowed to cover gaps between neighboring chips and fields. Median of the absolute values of the shifts were equal to 28.5 pixels in X axis and 29.2 pixels in Y axis for *I* filter (relative to selected image of given field with the best seeing). Corresponding values for *V* filter were equal to 31.5 and 25.4. Maximum shift values were equal to (220, 340) pixels in the *I*-band and (250, 240) pixels in the *V*-band.

All photometric measurements were corrected for chip "flatness" based on observations of standard Landolt (1992) stars set at various chip coordinates according to the description in Udalski *et al.* (2008a). Average number of observations per object is equal to 45 in each band but it varies significantly from field to field as shown in Fig. 1.

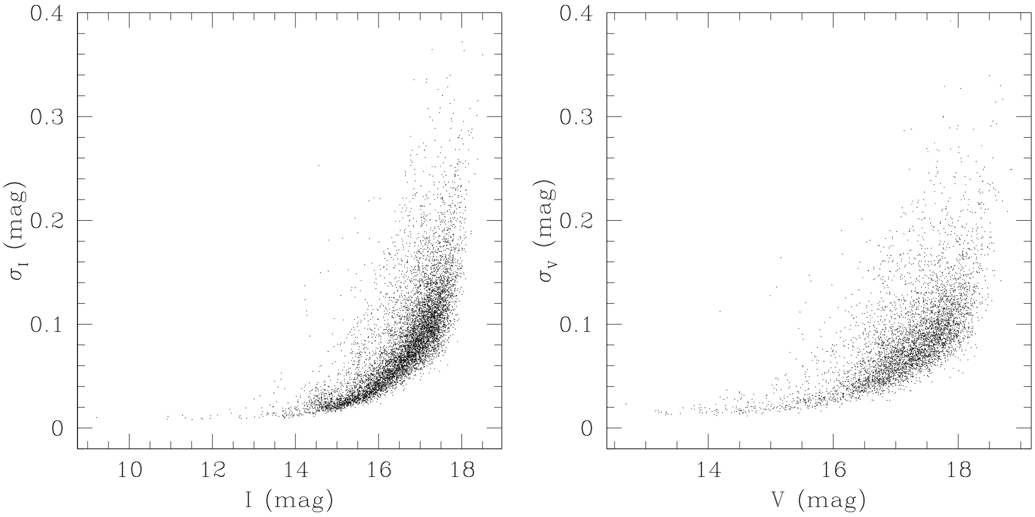

Fig. 2. Standard deviation of magnitudes for the LMC100.1 subfield

Photometric databases were constructed separately for each subfield (corresponding to one chip image) so some stars are present in multiple subfields.

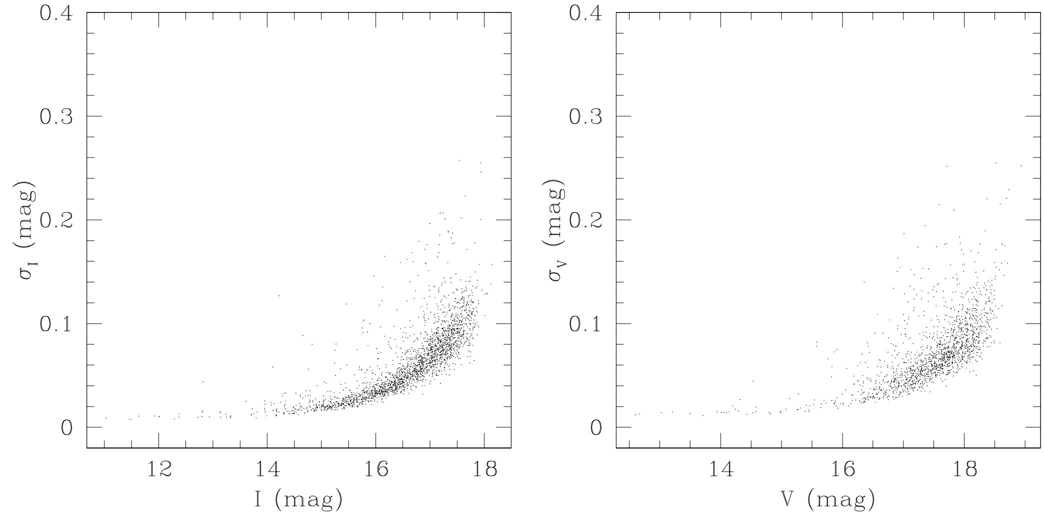

Fig. 3. Standard deviation of magnitudes for the LMC185.2 subfield

In order to check the quality of photometry we constructed diagrams shown in Figs. 2 and 3 presenting deviation of magnitudes as a function of magnitude for observations through both filters. The main goal of the survey was measuring stars brighter than 13 mag and as one can see the mean dispersion in *I*-band for such objects is significantly smaller than 0.02 mag.

4. Photometric and Astrometric Calibration

The same fields were observed as in the main OGLE-III survey so we were able to use the calibrated photometry and astrometry as a reference.

For each photometric subfield (2048×2068 pixels) the median value of photometric shifts for constant stars cross-correlated with the regular OGLE-III data was calculated with iterative 3σ clipping and all photometric measurements were appropriately adjusted. It was performed independently for observations in *I*- and *V*-bands. The accuracy of a zero-level point is within range 0.02–0.04 mag and shows dependency on star density in a given field. Figs. 4 and 5 present difference between standard OGLE-III photometry and shallow survey photometry as a function of chip coordinates – no significant correlation is visible.

The transformation of pixel coordinates to equatorial system was performed using equations derived through procedure described in Udalski *et al.* (2008a).

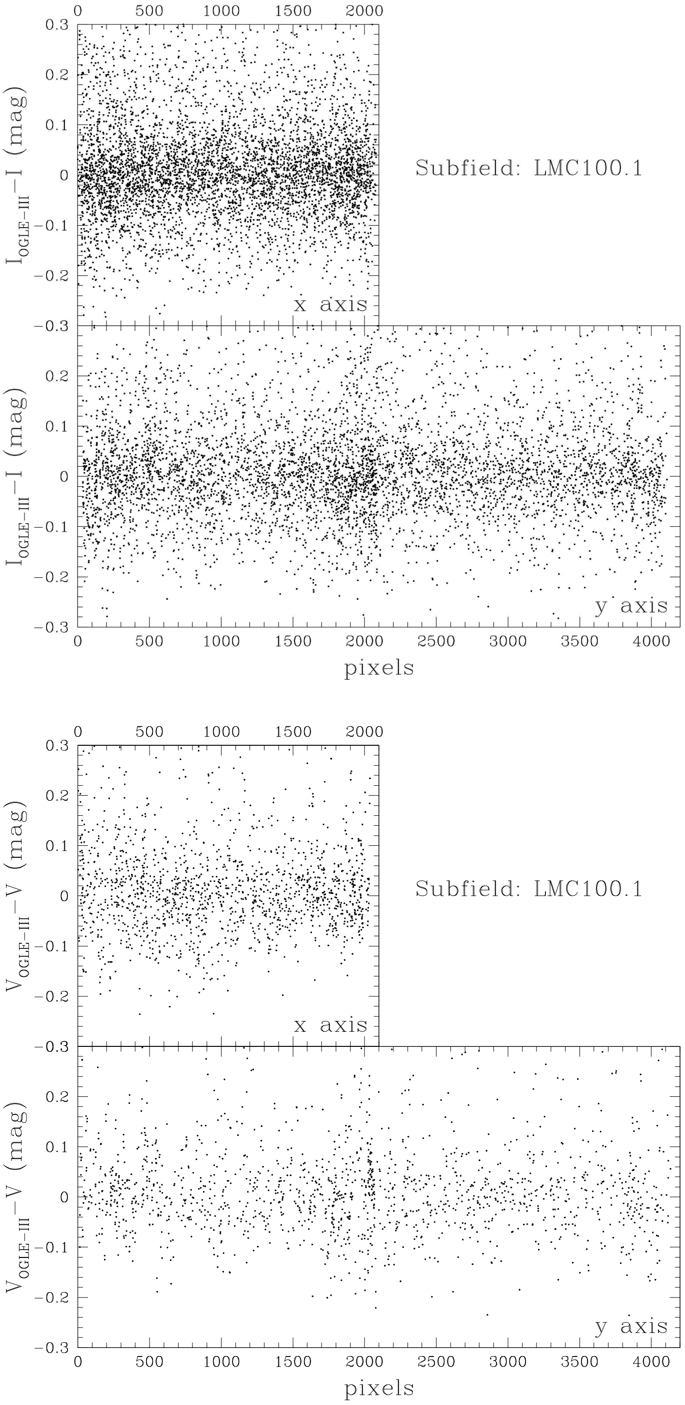

Fig. 4. Difference between standard OGLE-III calibrated photometry and shallow survey photometry in the *I*- and *V*-band for common stars from the central bar subfield LMC100.1. *Upper panels* show the difference as a function of X image coordinate (N–S direction) while the *lower panels* as a function of Y coordinate (E–W direction).

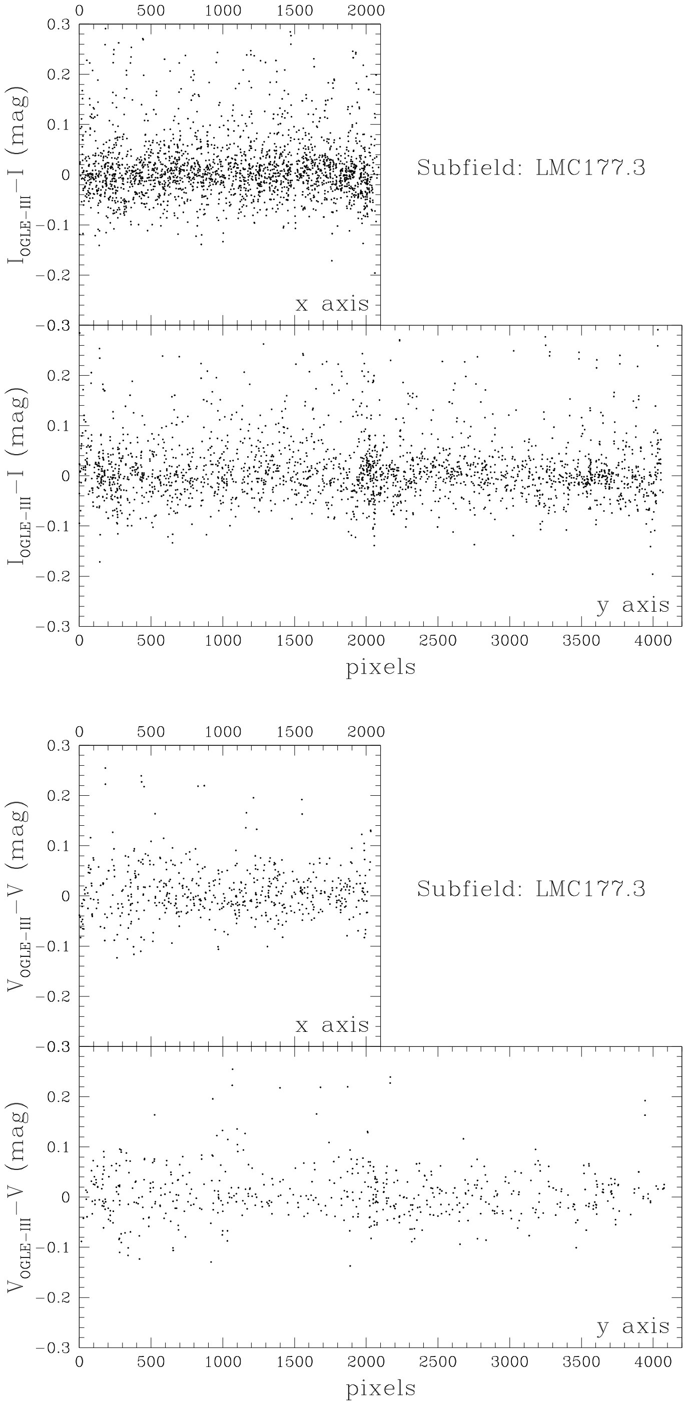

Fig. 5. Same as Fig. 4 for the LMC177.3 subfield.

5. Construction of Photometric Maps

The photometric databases were constructed separately for *I*- and *V*-band data thus the first step was cross-identification between objects registered in *I*- and *V*-band. A simple radius search was used and closest counterpart was selected if separation was less than 2.5 pixels, what corresponds to $0\farcs65$. Upper separation limit was selected in arbitrary way after calculating minimal distances between neighboring stars on single images.

For objects having at least 5 observations in each band 5σ deviating points were removed and magnitudes of all the remaining observational points were averaged. Next, the color term correction was applied for each object average magnitude according to the transformation equations and color term coefficients presented in Udalski *et al.* (2008a). During the conversion to the standard system the following formulae

$$\begin{aligned}(V-I) &= \frac{(v-i)}{(1-e_V+e_I)},\\ I &= i+e_I\cdot(V-I),\\ V &= v+e_V\cdot(V-I)\end{aligned}$$

were used, where v and i are instrumental magnitudes, while e_V and e_I are color term coefficients for corresponding filters.

As it was discussed in earlier papers (for example Udalski *et al.* 2002), the original calibration of the OGLE-III photometry was slightly inaccurate for very red or heavily reddened objects mainly due to the fact that the *I*-band filter used during the third phase of the project was not in full conformity with the standard Kron-Cousins definition (Landolt 1992). It showed quite wide transparency "wing" in the infrared part of the spectrum. Fortunately the OGLE-IV *I*-band filter can be practically considered the standard one so it was possible to compare red stars photometry with OGLE-III data and derive appropriate correction formula (Szymański *et al.* 2011):

$$\Delta I = -0.033918+0.016361(V-I)+0.004167(V-I)^2.$$

We used the above relation for correction of *I*-band photometry and $(V-I)$ color index for all objects with $(V-I)>1.5$ mag.

In the catalog we included interstellar extinction values obtained by Pejcha and Stanek (2009) based on RR Lyr variables and Haschke *et al.* (2012) based on red clump stars.

Table 2 presents the first 25 lines of the LMC photometric maps. The columns contain following data: (1) subfield designation, (2) ID number, (3,4) equatorial coordinates J2000.0, (5,6) corresponding X,Y pixel coordinates on the standard OGLE-III *I*-band reference image, (7,8,9) photometry: *I*, *V*, $V-I$, (10,11) number of points for average magnitude in *I*- and *V*-bands, (12,13) dispersion of magnitudes

Table 2

The first 25 lines of the LMC photometric maps based on the OGLE shallow survey

Field	ID	RA (J2000.0)	DEC (J2000.0)	x	y	I [mag]	V [mag]	$V-I$ [mag]	N_I	N_V	σ_I [mag]	σ_V [mag]	$N_I^{\rm bad}$	$N_V^{\rm bad}$	$E_{\rm RRLYR}(V-I)$ [mag]	$E_{\rm RC}(V-I)$ [mag]	A_I [mag]	$\rm ID_{OGLEIII}$
LMC100.1	s1	$5^h19^m53.3^s$	$-69^\circ27'34''$	1373.3	1016.2	10.383	12.346	1.964	64	59	0.095	0.183	0	0	0.125	0.020	0.028	–
LMC100.1	s2	$5^h20^m16.2^s$	$-69^\circ30'04''$	792.0	1473.3	10.510	11.430	0.921	64	56	0.010	0.017	0	0	0.101	0.030	0.042	–
LMC100.1	s3	$5^h20^m38.3^s$	$-69^\circ30'05''$	784.3	1919.4	10.960	11.516	0.555	65	61	0.011	0.014	0	0	0.101	0.030	0.042	–
LMC100.1	s4	$5^h19^m32.1^s$	$-69^\circ25'33''$	1837.1	592.2	11.150	13.181	2.031	42	46	0.033	0.074	0	0	0.125	0.030	0.042	–
LMC100.1	s5	$5^h19^m49.6^s$	$-69^\circ30'04''$	796.6	939.3	11.264	12.145	0.882	62	56	0.167	0.052	0	0	0.126	0.030	0.042	–
LMC100.1	s6	$5^h19^m56.8^s$	$-69^\circ26'13''$	1680.3	1089.9	11.378	11.936	0.558	64	58	0.010	0.016	0	0	0.125	0.020	0.028	–
LMC100.1	s7	$5^h19^m50.2^s$	$-69^\circ26'50''$	1542.5	955.9	11.500	13.410	1.910	63	58	0.019	0.040	0	0	0.125	0.020	0.028	–
LMC100.1	s8	$5^h19^m51.9^s$	$-69^\circ29'15''$	985.2	985.7	11.548	12.259	0.712	62	58	0.008	0.016	0	0	0.126	0.030	0.042	–
LMC100.1	s9	$5^h20^m33.8^s$	$-69^\circ32'35''$	206.9	1823.2	11.640	11.614	-0.026	39	24	0.025	0.020	0	0	0.101	0.030	0.042	–
LMC100.1	s10	$5^h19^m56.9^s$	$-69^\circ26'39''$	1581.0	1091.4	11.760	12.303	0.542	64	58	0.010	0.016	0	0	0.125	0.020	0.028	–
LMC100.1	s11	$5^h19^m55.3^s$	$-69^\circ28'37''$	1131.0	1055.9	11.803	12.540	0.737	64	58	0.009	0.016	0	0	0.125	0.020	0.028	–
LMC100.1	s12	$5^h20^m06.2^s$	$-69^\circ30'02''$	801.7	1273.5	12.012	13.281	1.269	63	58	0.009	0.017	0	0	0.126	0.040	0.056	–
LMC100.1	s13	$5^h19^m24.2^s$	$-69^\circ25'46''$	1789.6	431.6	12.044	13.711	1.667	42	40	0.017	0.021	0	0	0.125	0.030	0.042	–
LMC100.1	s14	$5^h19^m44.4^s$	$-69^\circ25'43''$	1799.4	840.0	12.206	13.824	1.618	59	59	0.012	0.018	0	0	0.125	0.020	0.028	–
LMC100.1	s15	$5^h19^m18.9^s$	$-69^\circ31'08''$	554.7	318.7	12.316	14.120	1.804	47	32	0.018	0.030	0	0	0.126	0.060	0.085	–
LMC100.1	s16	$5^h19^m41.0^s$	$-69^\circ24'45''$	2022.7	772.4	12.388	14.180	1.792	46	51	0.016	0.028	0	0	0.125	0.020	0.028	–
LMC100.1	s17	$5^h20^m39.0^s$	$-69^\circ32'48''$	157.9	1927.7	12.510	14.211	1.701	59	54	0.018	0.022	0	1	0.101	0.030	0.042	–
LMC100.1	s18	$5^h19^m44.0^s$	$-69^\circ30'53''$	608.7	825.0	12.926	16.563	3.637	56	49	0.168	0.434	0	0	0.126	0.030	0.042	–
LMC100.1	s19	$5^h19^m32.5^s$	$-69^\circ30'35''$	678.9	592.6	12.849	15.255	2.406	54	55	0.049	0.090	0	0	0.126	0.040	0.056	LMC100.1.21
LMC100.1	s20	$5^h19^m23.9^s$	$-69^\circ27'11''$	1464.5	424.5	12.906	14.446	1.541	59	56	0.009	0.013	0	0	0.125	0.030	0.042	LMC100.1.75626
LMC100.1	s21	$5^h19^m09.1^s$	$-69^\circ25'55''$	1755.8	125.2	13.082	15.393	2.311	56	54	0.028	0.077	0	0	0.125	0.070	0.099	LMC100.1.75615
LMC100.1	s22	$5^h20^m08.8^s$	$-69^\circ32'16''$	287.0	1320.4	13.047	16.914	3.866	47	29	0.140	0.263	0	0	0.126	0.040	0.056	LMC100.1.19270
LMC100.1	s23	$5^h19^m27.8^s$	$-69^\circ30'30''$	697.5	498.3	12.957	13.975	1.018	55	54	0.098	0.157	0	0	0.126	0.040	0.056	LMC100.1.19
LMC100.1	s24	$5^h19^m39.4^s$	$-69^\circ25'27''$	1859.6	739.1	12.985	16.778	3.793	45	39	0.290	0.604	0	0	0.125	0.020	0.028	–
LMC100.1	s25	$5^h19^m33.5^s$	$-69^\circ30'18''$	744.0	612.7	13.140	14.694	1.554	56	56	0.125	0.176	0	0	0.126	0.040	0.056	LMC100.1.23

for *I*- and *V*-bands, (14,15) number of 5σ removed points in *I*- and *V*-bands, (16-18) extinction values for given object coordinates, (19) ID number of cross-identified star in the standard OGLE-III database. "+" mark before designation in column (19) indicates multiple cross-identification (closest star was used in Table 2).

6. Discussion

The data from the shallow survey presented in this paper extend already published, detailed OGLE-III photometric maps for Large Magellanic Cloud into the brighter magnitudes domain. We were able to obtain photometry for objects as bright as 9.1 mag. Fig. 6 shows positions of all stars brighter than 14.5 mag – the structure of the galaxy can be easily recognized.

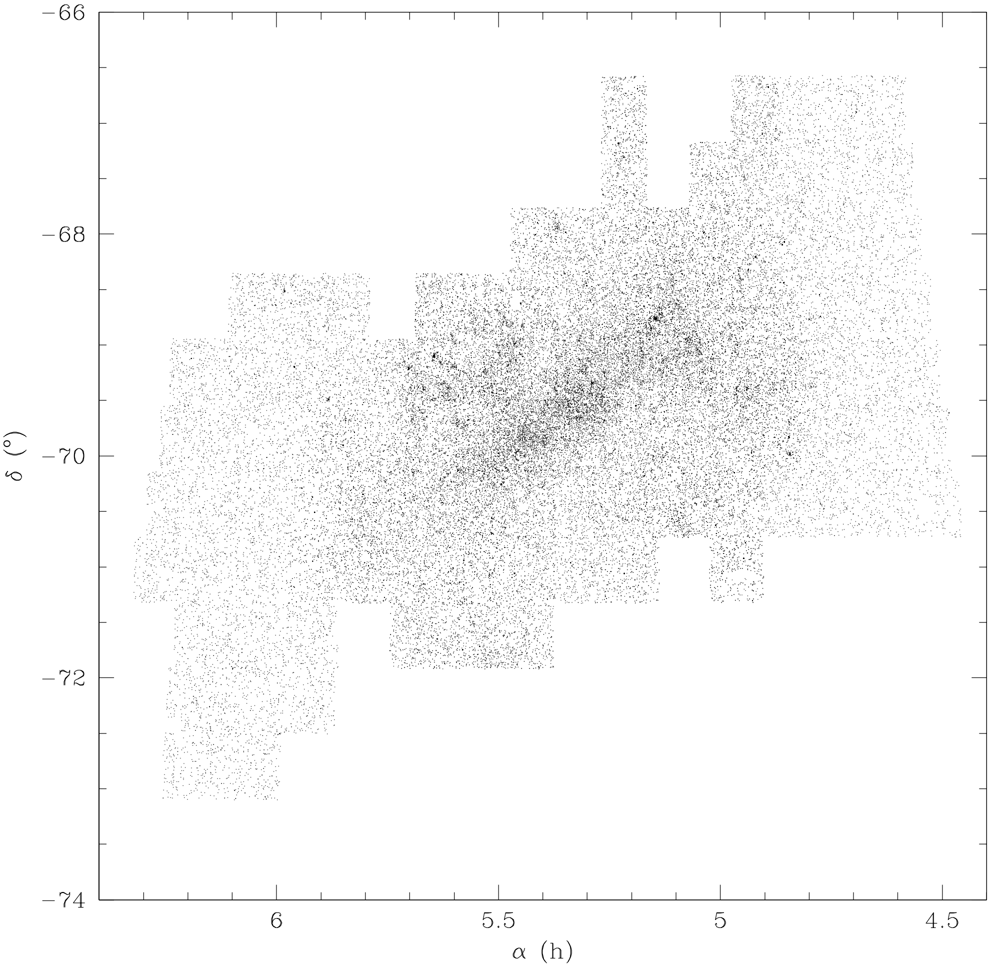

Fig. 6. Positions of all stars brighter than 14.5 mag in the observed fields after removal of doubled objects from neighboring subchips/fields.

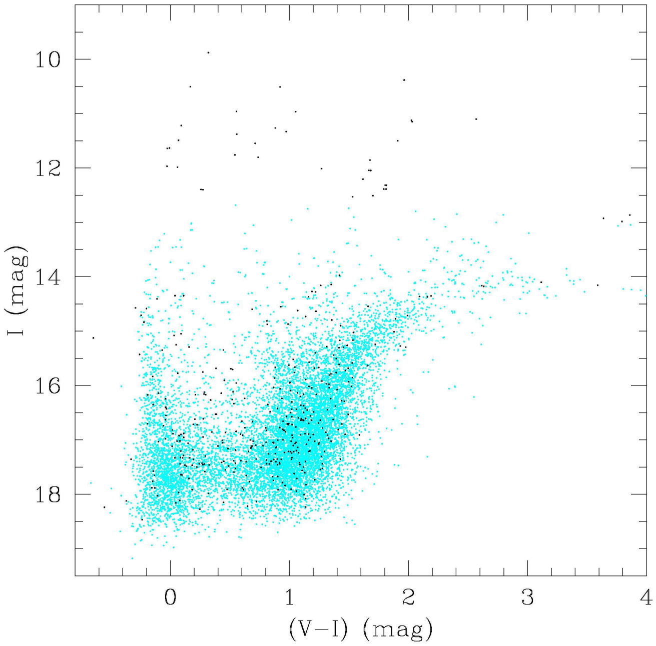

Fig. 7. Color–magnitude diagram for the LMC100.1 subfield. The black points represent stars for which no corresponding objects were found in the standard OGLE-III data.

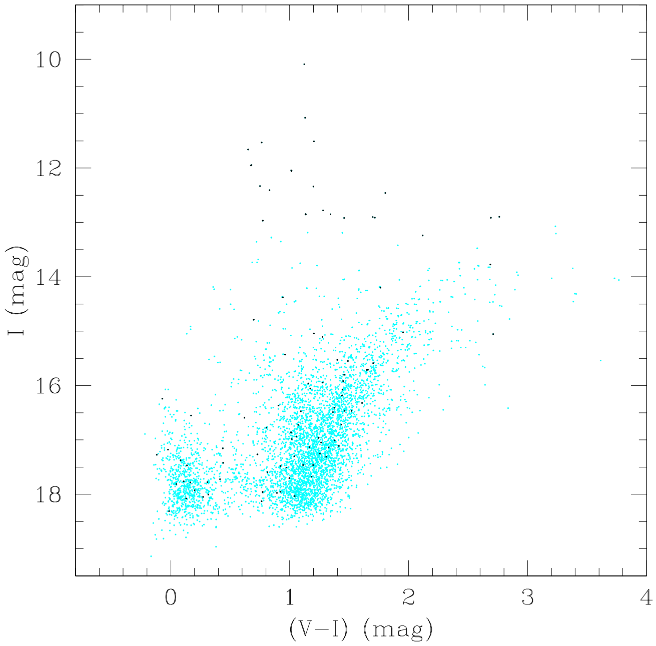

Fig. 8. Color–magnitude diagram for the LMC185.2 subfield. The black points represent stars for which no corresponding objects were found in the standard OGLE-III data.

Figs. 7 and 8 present the color–magnitude diagrams based on photometric maps for the LMC100.1 and LMC185.2 subfields. Corresponding histograms of magnitudes in both bands are shown in Figs. 9 and 10. It is worth noting that apart of bright stars we could also obtain completely new photometry for many fainter stars (78 154 objects) located close to saturated objects in the main OGLE-III survey data. Area around such objects had to be masked on the reference images in order to ensure high effectiveness of automatic DIA pipelines and avoid artifact detections in this massive photometry survey. We prepared the list with coordinates of such objects that will allow to obtain more precise PSF photometry from regular OGLE-III images. There is also a significant number of newly found stars (17 480) which are located outside OGLE-III template images. This is due to the fact that the OGLE-III photometry is based on reference images which are stacked from several images registered during the best photometric nights while in the shallow survey no reference images were constructed and the complete sample of objects detected on all frames was used in the analysis. As it was mentioned before, subsequent images of the same field were sometimes considerably shifted what allowed to broaden the "field of view" in the observed fields.

Table 3 summarizes obtained photometry for all objects. In the subsequent columns following data are presented: (1) OGLE-III field name, (2) number of objects for which photometry is available in the main OGLE-III photometric maps, (3) total number of objects in the shallow survey photometric maps for given field, (4) number of new objects (not present in the main OGLE-III photometric maps) for given field, (5) number of new objects brighter in the I-band than brightest star for given field in the main OGLE-III photometric maps, (6) same as (5) but for the V-band, (7) number of new objects brighter in the I-band and V-band than brightest stars in the corresponding bands for given field in the main OGLE-III photometric maps.

To show quality of obtained PSF photometry we present comparison of light curves for some unblended Cepheid variables to the standard OGLE-III and ASAS (Pojmański 1997 and 2002) data (Figs. 11–17). As one can see despite the weather was much worse than during usual observational conditions the quality of photometry turned out to be good. Obviously, for some non-isolated stars one can expect significant blending due to blurred stellar profiles.

Beside the OGLE LMC mapping several other photometric surveys have been conducted for the LMC. They based usually on one/few-epoch data what limited possible apllications of these studies. Cioni *et al.* (2000) presented point sources catalog (ca. 1.3 million objects) from the DENIS survey carried out using I, J and K_S filters and consisting of objects for which $10.5~\mathrm{mag} < I < 18~\mathrm{mag}$. *UBVR* catalog of 179 655 stars within $V = 12 \div 18$ mag range was presented by Massey (2002). However in that case the galaxy was not fully covered. Finally, Zaritsky *et al.* (2004) used Johnson U, B, V and Gunn i filters to obtain photometry for 24 million stars in the LMC with brightness of $13.5 \div 20$ mag in the V-band.

Table 3

Summary of the number of objects in the LMC fields

Field	N_{OIII}	N	N_{NEW}	N_I	N_V	N_{VI}	Field	N_{OIII}	N	N_{NEW}	N_I	N_V	N_{VI}
LMC100	1075711	78189	2087	109	59	49	LMC155	71173	1513	100	45	34	34
LMC101	548707	33906	1067	45	27	27	LMC156	72805	1497	92	57	43	43
LMC102	266963	17906	694	40	48	38	LMC157	44165	1652	165	58	43	43
LMC103	833034	70973	4999	86	47	42	LMC158	34264	1106	51	37	29	29
LMC104	549136	34840	5067	57	40	40	LMC159	234254	16484	381	104	48	48
LMC105	353469	24324	419	106	39	39	LMC160	437897	27916	466	172	72	72
LMC107	226287	13997	591	135	45	45	LMC161	787467	58273	1388	151	75	73
LMC108	257801	14467	664	234	67	67	LMC162	1171172	81387	2551	128	51	51
LMC109	294145	18112	408	31	21	21	LMC163	806912	48609	12864	95	50	50
LMC110	529605	39037	2068	49	47	41	LMC164	381352	25569	747	75	50	50
LMC111	696121	48742	1997	77	32	32	LMC165	329028	20376	509	80	40	40
LMC112	752907	29773	7666	115	50	48	LMC167	394585	26472	628	135	49	49
LMC113	561679	25119	380	117	67	67	LMC168	636559	44717	1108	230	119	103
LMC114	221912	15669	1198	66	46	46	LMC169	1092986	65398	1273	155	63	63
LMC117	527346	21419	2394	143	68	68	LMC170	878425	55419	1084	155	79	79
LMC118	694697	39844	1824	48	50	39	LMC171	513519	28705	2077	116	34	34
LMC119	817851	46299	2083	186	60	60	LMC172	423099	22182	771	91	62	62
LMC120	617701	30819	371	104	38	38	LMC174	340208	14762	1638	130	52	52
LMC121	442352	31664	778	113	76	65	LMC175	497977	23122	1617	402	205	204
LMC124	290411	18125	621	74	50	50	LMC176	576984	22129	1968	150	85	84
LMC125	357288	21252	640	70	50	33	LMC177	817966	26121	613	108	63	63
LMC126	530735	30877	897	31	59	25	LMC178	471477	18525	2964	91	52	52
LMC127	547901	35676	2473	166	57	57	LMC179	296759	13925	550	70	51	51
LMC128	406243	25285	675	30	51	26	LMC183	361838	18671	1566	156	71	71
LMC129	304616	20516	1387	68	46	36	LMC184	486666	24001	524	129	65	64
LMC130	231039	13949	1615	137	41	41	LMC185	630366	32496	705	147	80	80
LMC131	248421	8279	364	136	42	42	LMC186	376966	28750	2662	65	48	47
LMC132	217827	7998	147	59	21	21	LMC189	153656	3784	256	70	46	46
LMC133	346558	16403	1976	237	112	112	LMC190	200564	5106	904	78	34	34
LMC134	304271	18835	300	52	43	38	LMC191	243558	10646	951	148	76	72
LMC135	284846	20805	2808	146	54	50	LMC192	228516	10391	611	110	101	93
LMC136	244490	19405	2673	74	20	15	LMC193	138223	9098	480	74	77	74
LMC137	200058	5965	539	61	24	24	LMC194	77816	2941	69	30	34	27
LMC138	117664	3076	369	22	17	17	LMC195	43002	2088	327	36	30	30
LMC139	128858	4141	226	36	24	24	LMC196	116258	4373	108	18	19	16
LMC140	188164	5050	103	46	34	34	LMC197	92295	3769	116	36	28	28
LMC141	191197	5660	247	54	36	35	LMC198	71992	3488	223	56	37	37
LMC142	225807	6808	940	81	36	36	LMC199	63841	3154	144	34	25	25
LMC143	155672	5329	330	52	24	24	LMC200	58765	3013	193	30	24	24
LMC144	116363	3481	508	29	24	24	LMC201	91051	2254	362	81	57	57
LMC145	64628	1902	222	18	19	17	LMC202	79469	2158	175	62	55	55
LMC146	86656	2621	240	20	21	17	LMC203	71396	1964	201	44	48	42
LMC147	103604	3105	167	43	31	29	LMC204	108173	3085	118	72	48	48
LMC148	110885	3000	290	40	39	35	LMC205	82072	2755	185	48	28	28
LMC149	115117	3448	268	32	31	28	LMC206	78179	2357	364	43	43	41
LMC150	96039	3119	100	16	27	16	LMC207	70889	2036	68	22	27	21
LMC151	89935	2403	170	35	22	22	LMC208	87619	2046	98	69	54	54
LMC152	46107	1468	96	63	56	56	LMC209	64885	1737	81	23	53	22
LMC153	56016	1565	92	49	40	40	LMC210	70282	1610	97	8	28	7
LMC154	65095	1635	61	32	31	30	LMC211	61205	1473	50	46	29	29
LMC155	71173	1513	100	45	34	34	LMC212	81878	2017	54	19	23	18
LMC156	72805	1497	92	57	43	43	LMC213	52207	1926	111	44	48	44
LMC157	44165	1652	165	58	43	43	LMC214	60410	1661	108	23	23	22
LMC158	34264	1106	51	37	29	29	LMC215	60801	1236	58	29	20	20

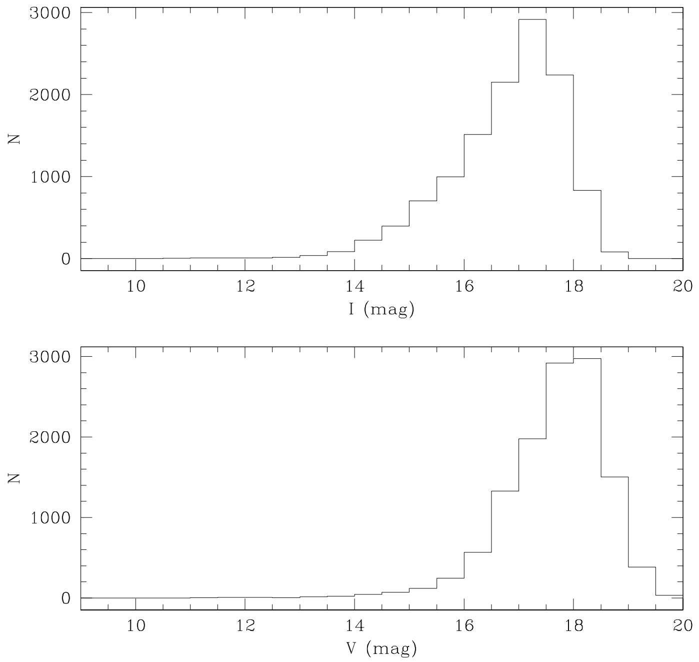

Fig. 9. Histogram of magnitudes for the LMC100.1 subfield

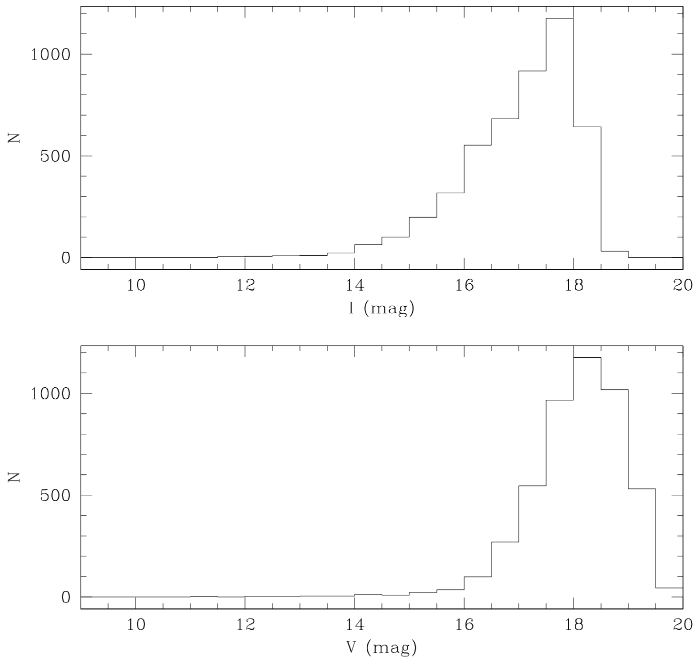

Fig. 10. Histogram of magnitudes for the LMC185.2 subfield

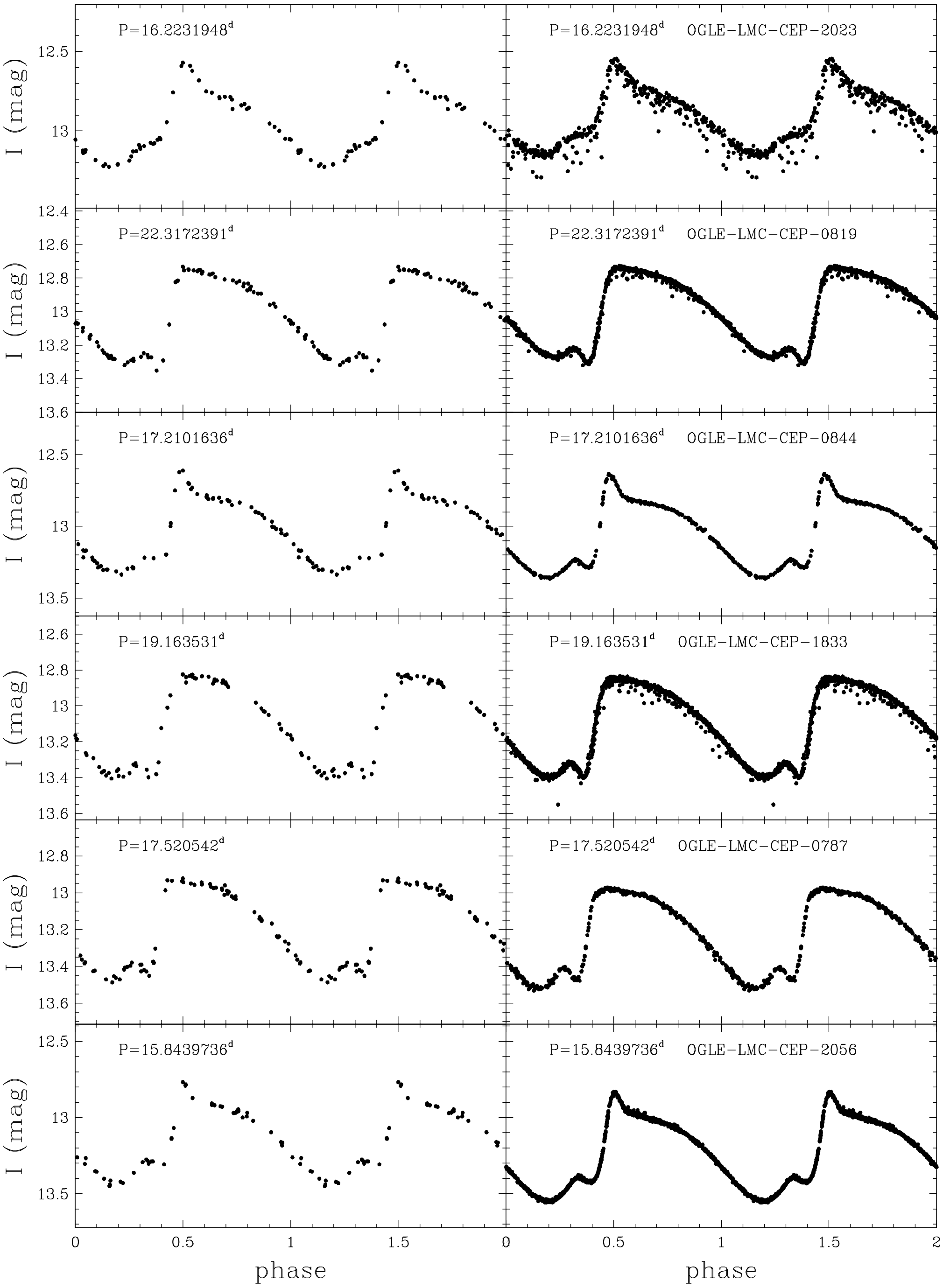

Fig. 11. Comparison of shallow survey *I*-band light curves of classical Cepheids in the LMC (*left panels*) with the standard OGLE-III data (*right panels*).

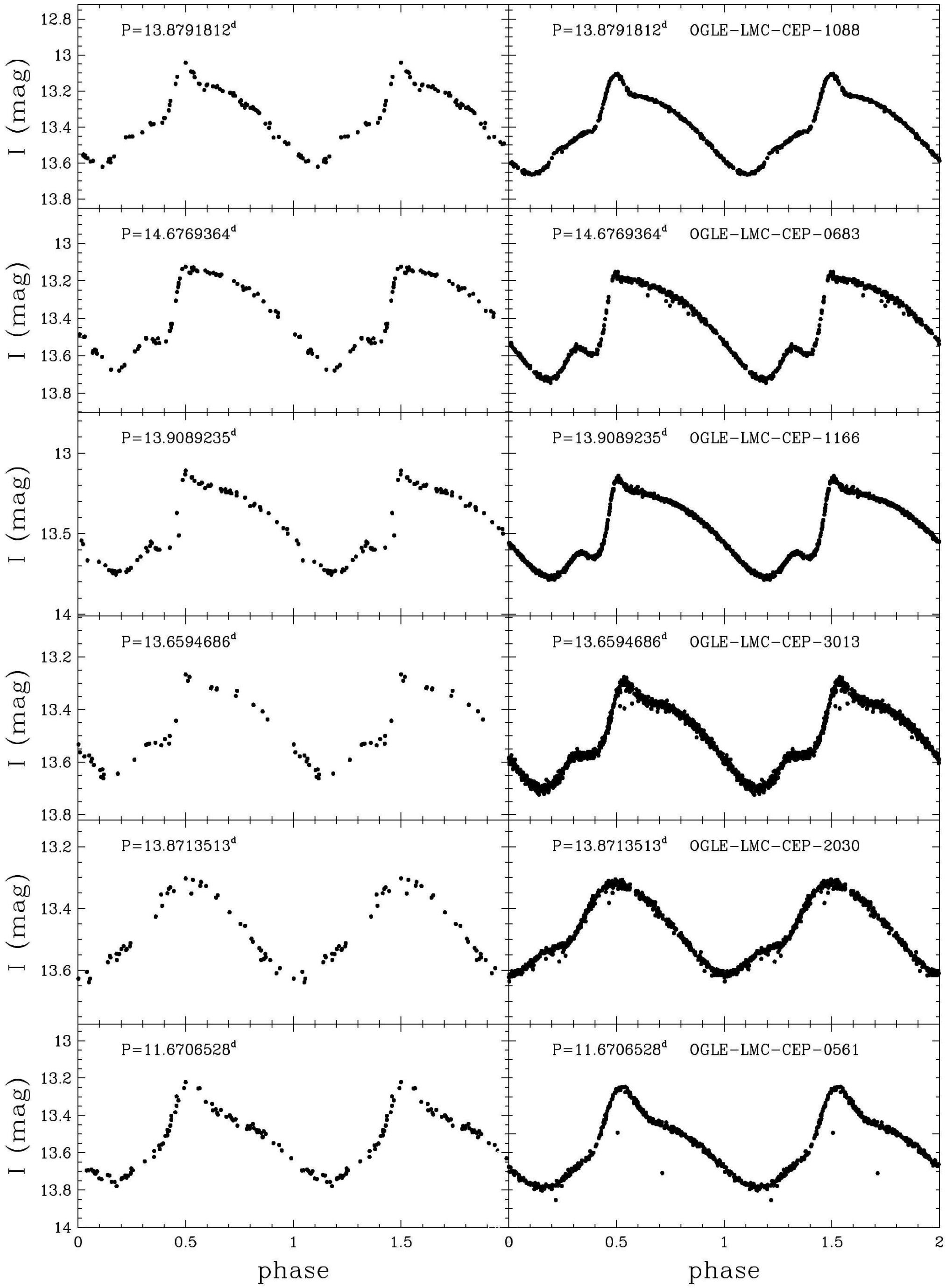

Fig. 12. Same as in Fig. 11.

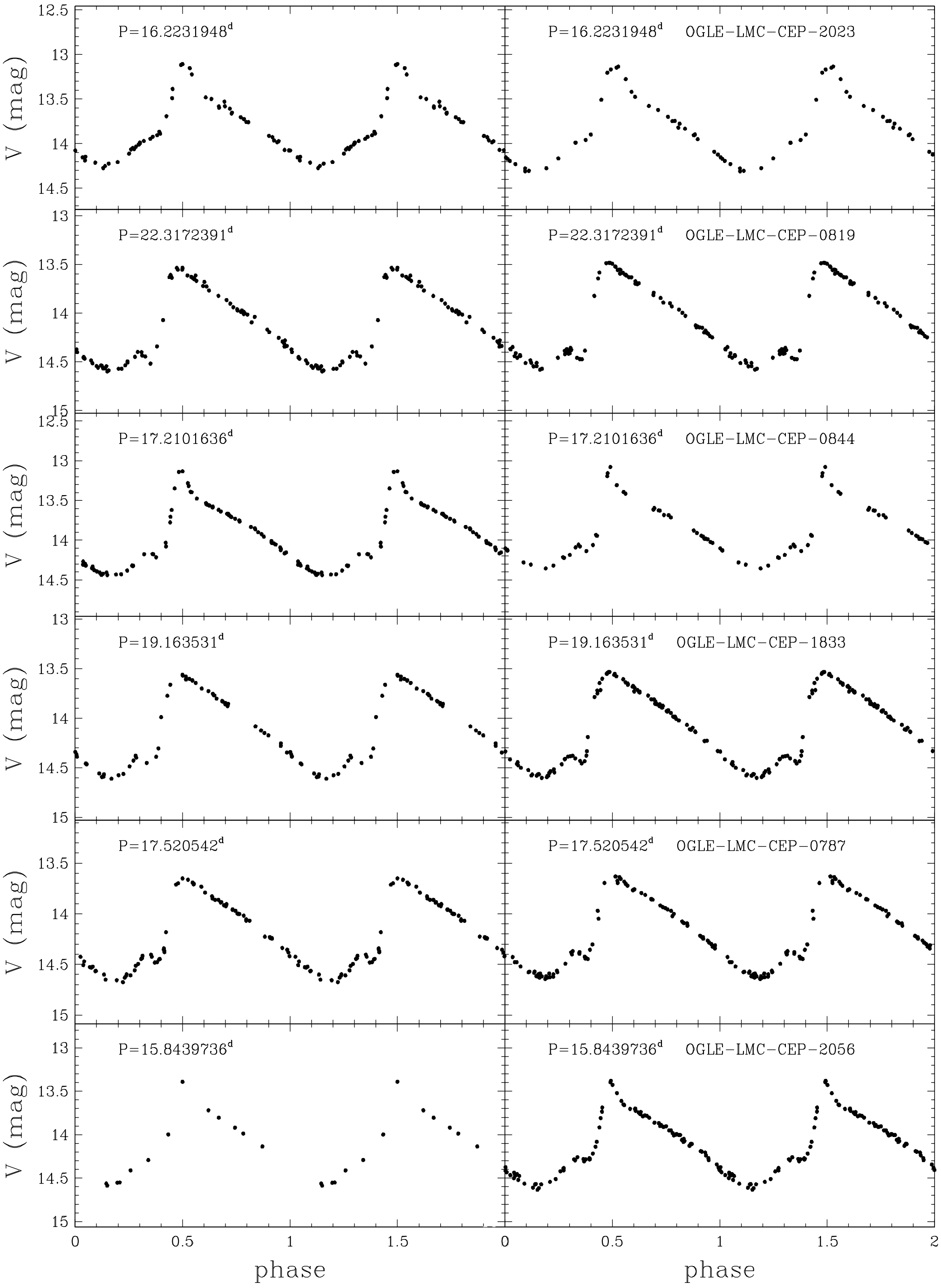

Fig. 13. Comparison of shallow survey *V*-band light curves of classical Cepheids in the LMC (*left panels*) with the standard OGLE-III data (*right panels*) for the same objects as in Fig. 11.

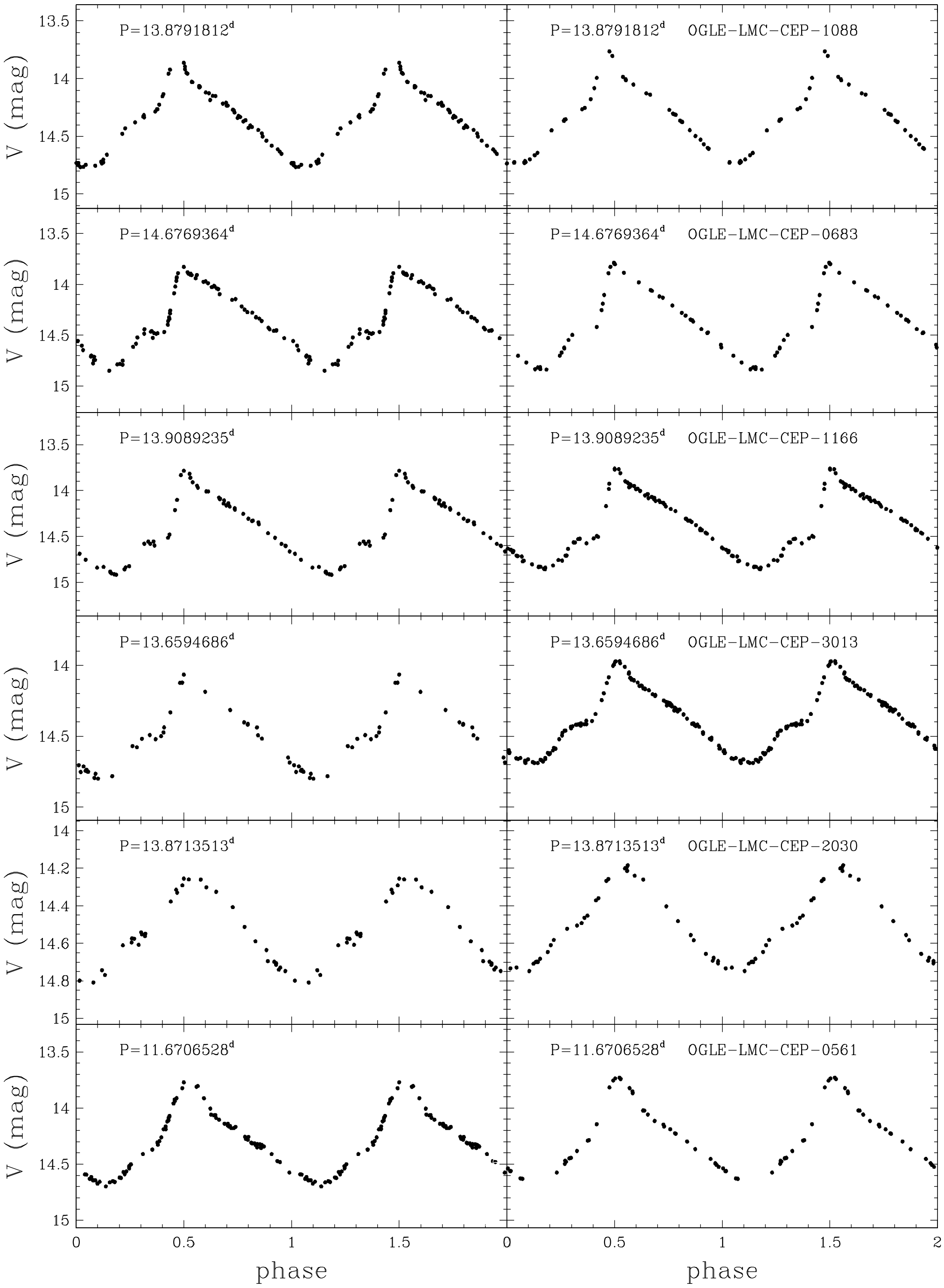

Fig. 14. Comparison of shallow survey *V*-band light curves of classical Cepheids in the LMC (*left panels*) with the standard OGLE-III data (*right panels*) for the same objects as in Fig. 12.

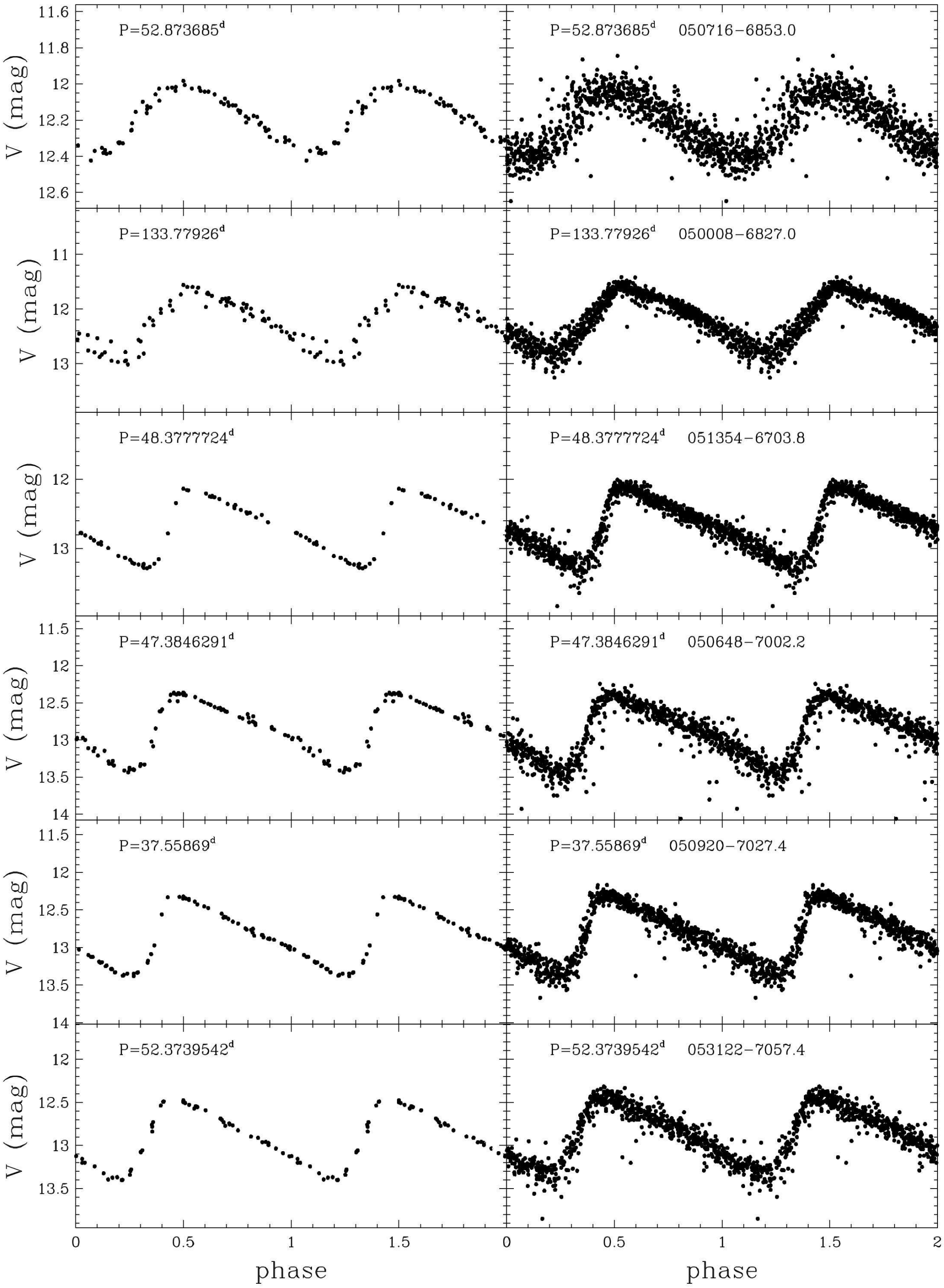

Fig. 15. Comparison of light curves of classical Cepheids in the LMC in the *V*-band with the ASAS data (*right panels*).

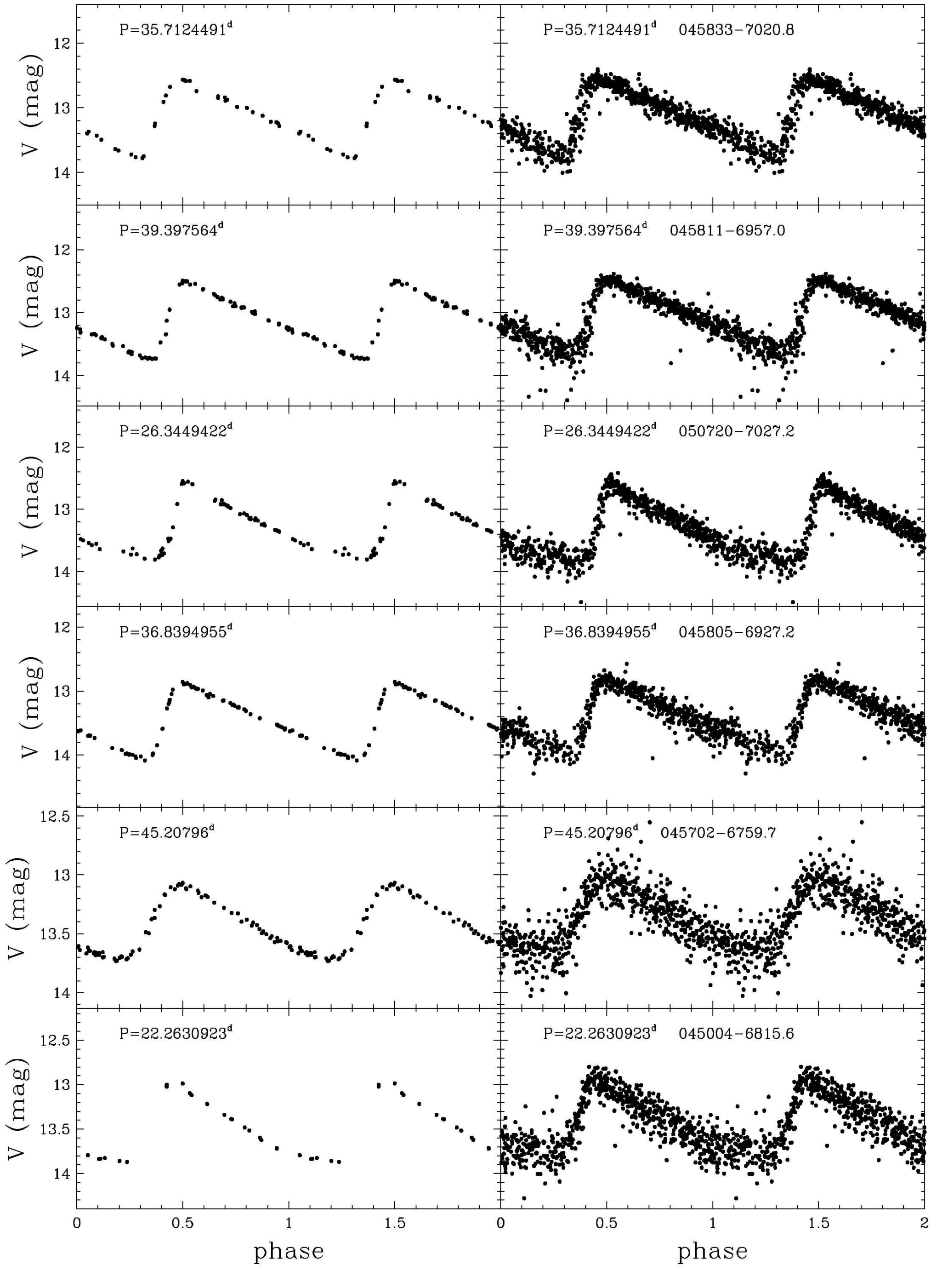

Fig. 16. Same as in Fig. 15.

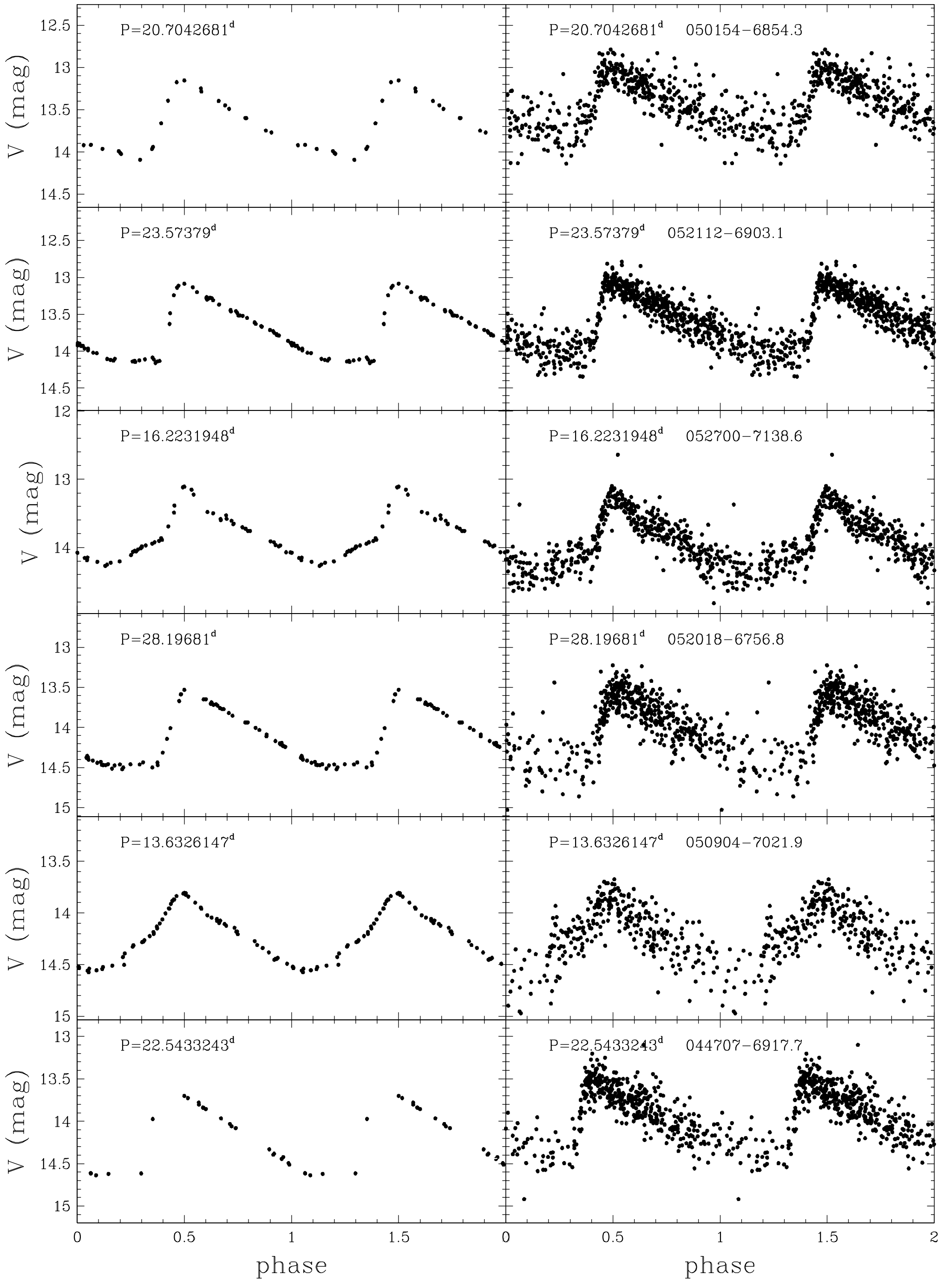

Fig. 17. Same as in Fig. 15.

In the forthcoming paper we will present results of variability analysis performed for all new objects. For the Small Magellanic Cloud complete sets of short-exposure images were also collected and we plan to publish similar data for this galaxy.

7. Data Availability

The photometric maps for bright objects in the LMC are available to the astronomical community from the OGLE Internet Archive:

http://ogle.astrouw.edu.pl
ftp://ftp.astrouw.edu.pl/ogle3/maps/lmc_bright/

Acknowledgements. The OGLE project has received funding from the European Research Council under the European Community's Seventh Framework Programme (FP7/2007-2013)/ERC grant agreement no. 246678 to AU. This paper was partially supported by Polish grant N N203 510038. We gratefully acknowledge financial support for this work from the Chilean Center for Astrophysics FONDAP 15010003, and from the BASAL Centro de Astrofisica y Tecnologias Afines (CATA) PFB-06/2007.

REFERENCES

Cioni, M.-R., *et al.* 2000, *A&AS*, **144**, 235.
Haschke, R., Grebel, E.K., and Duffau, S. 2011, *AJ*, **141**, 158.
Landolt, A.U. 1992, *AJ*, **104**, 372.
Massey, P. 2002, *ApJS*, **141**, 81.
Pejcha O., and Stanek, K.Z. 2009, *ApJ*, **704**, 1730.
Pojmański, G. 1997, *Acta Astron.*, **47**, 467.
Pojmański, G. 2002, *Acta Astron.*, **52**, 397.
Stetson, P.B. 1987, *PASP*, **99**, 191.
Szymański, M., Udalski, A., Soszyński, I., Kubiak, M., Pietrzyński, G., Poleski, R., Wyrzykowski, Ł., and Ulaczyk, K. 2011, *Acta Astron.*, **61**, 83.
Udalski, A., Szymański, M., Kubiak, M., Pietrzyński, G., Soszyński, I., Woźniak, P., Żebruń, K., Szewczyk, O., and Wyrzykowski, Ł. 2002, *Acta Astron.*, **52**, 217.
Udalski, A. 2003, *Acta Astron.*, **53**, 291.
Udalski, A., Szymański, M., Soszyński, I., and Poleski, R. 2008a, *Acta Astron.*, **58**, 69.
Udalski, A., Soszyński, I., Szymański, M., Kubiak, M., Pietrzyński, G., Wyrzykowski, Ł, Szewczyk, O., Ulaczyk, K. and Poleski, R. 2008b, *Acta Astron.*, **58**, 89.
Zaritsky, D., Harris, J., Thompson, I., and Grebel, E.K. 2004, *AJ*, **128**, 1606.